Frontiers of Information Technology & Electronic Engineering
www.jzus.zju.edu.cn; engineering.cae.cn; www.springerlink.com
ISSN 2095-9184 (print); ISSN 2095-9230 (online)
E-mail: jzus@zju.edu.cn

Entropy-statistical approach to phase-locking detection of oscillations*

Petr BORISKOV‡, Vadim PUTROLAYNEN, Andrei VELICHKO, Kristina PELTONEN

Institute of Physics and Technology, Petrozavodsk State University, Petrozavodsk 185910, Russia

E-mail: boriskov@petrsu.ru; vputr@petrsu.ru; velichkogf@gmail.com; krispelt@yandex.ru

Received June 11, 2025; Revision accepted Nov. 13, 2025; Crosschecked Dec. 3, 2025

Abstract: This study proposes a method for analyzing synchronization in oscillator systems, illustrated by modeling the dynamics of a circuit of two resistively coupled pulse oscillators. The dynamic characteristic of synchronization is the fuzzy entropy (FuzzyEn), which is calculated from a time series composed of the ratios of the number of pulse periods (subharmonic ratio, SHR) at phase-locking intervals. Low and high entropy values indicate strong and weak synchronization between the two oscillators, respectively. The proposed method effectively visualizes synchronized modes of the circuit using entropy maps of synchronization states. In addition, a classification of synchronization states is proposed based on the dependency of FuzzyEn on the embedding vector length of the SHR time series. An extension of this method for analyzing non-pulse (non-spike) signals is demonstrated using the example of phase–phase coupling rhythms of the local field potential of the rat hippocampus. The proposed entropy-statistical approach, using integers and pulse signal forms, is well-suited for signal synchronization analysis and can be implemented on digital mobile platforms.

Key words: Pulse oscillations; Phase locking; High-order synchronization; Subharmonic ratio; Fuzzy entropy; Hilbert transform
https://doi.org/10.1631/FITEE.2500402 **CLC number:** TN911.7

1 Introduction

Synchronization is a fundamental phenomenon that plays a critical role in various fields of science and technology (Pikovsky et al., 2002; Park et al., 2003; Belluscio et al., 2012; Nikonov et al., 2015; Lowet et al., 2016). For example, in all digital communication systems, synchronization is essential for establishing precise phase relationships between the transmission and reception cycles of digital signals (Park et al., 2003). In neurophysiology, neuronal oscillatory synchronization is the basis for information coordination between cortical neural networks (Belluscio et al., 2012; Lowet et al., 2016).

A new direction in neural network technologies, known as oscillator computing, is entirely based on the effect of synchronization (Nikonov et al., 2015; Romera et al., 2018; Chou et al., 2019; Wang and Roychowdhury, 2019; Mallick et al., 2020). For example, the ability to perform vowel classification using the frequency synchronization characteristics of four coupled spin-torque nano-oscillators has been demonstrated (Romera et al., 2018). Chou et al. (2019) and Wang and Roychowdhury (2019) solved the max-cut problem using the synchronization of tank oscillators.

The regular or irregular nature of dynamics in many applied tasks indicates the “correct” or “incorrect” system operation, respectively. Examples include jitter in digital devices, which is a primary source of

‡ Corresponding author

* Project supported by the Russian Science Foundation (No. 22-11-00055-P)

ORCID: Petr BORISKOV, https://orcid.org/0000-0002-2904-9612; Vadim PUTROLAYNEN, https://orcid.org/0000-0001-5707-7760; Andrei VELICHKO, https://orcid.org/0000-0002-9341-1831; Kristina PELTONEN, https://orcid.org/0009-0004-3584-6142

distortion in frequency synthesizers (Li et al., 2023), anomalies in electrocardiograms (Ramírez et al., 2024), irregularities in the rotational speed of gears and motors (Bonet-Jara et al., 2021; Cui et al., 2024), and irregularities in earthquake precursors (Biagi et al., 2001). Signal regularity is typically assessed by calculating the signal entropy, such as fuzzy (Ishikawa and Mieno, 1979), sample (Delgado-Bonal and Marshak, 2019), or singular value decomposition (Alter et al., 2000) entropy indicators. The synchronization of oscillations in interacting systems is closely related to the regularity of their joint dynamics. Therefore, entropy calculation is a promising approach for detecting and analyzing oscillation synchronization.

The phase-locking parameter (PLP) is one of the most commonly used characteristics of signal synchronization (Pikovsky et al., 2002; Belluscio et al., 2012; Lowet et al., 2016):

$$P_{nm}=\frac{1}{T}\left|\sum_{t=1}^{T}\exp\left(\mathrm{i}\Delta\varphi_{nm}(t)\right)\right|, \tag{1}$$

where $\Delta\varphi_{nm}(t)$ denotes the phase difference between signals with integers n and m (see Eq. (2) in Section 2.3), and T represents the total number of time points in the sample. The PLP is a set of integral characteristics computed from several samples for different n and m. The result of these calculations is the classification of the system as likely synchronized or unsynchronized for a given n and m. Spectral coherence is another signal synchronization metric. This is the most comprehensive assessment of synchronization (Lowet et al., 2016); however, it requires the calculation of spectra and the mutual correlation function of signals, making it as complex as the PLP. Thus, a simple and effective method for signal synchronization estimation can be easily implemented on mobile digital platforms (microcontrollers, etc.) with low computing resources being urgently required.

In our recent work (Boriskov et al., 2024), we proposed the concept of estimating phase-locking pulse signals based on the calculation of the entropy of a time series of subharmonic ratio (SHR) coefficients (Velichko et al., 2018a, 2018b). The SHR of two pulse signals is the ratio of the numbers of their periods in intervals between pulse coincidences, and the phase-locking metric reflects synchronization efficiency (SE), which is based on the SHR of the time series. Based on these metrics, a new type of spike neural networks (Velichko et al., 2018a; Velichko, 2019) with high-order synchronization (HOS) effects is developed. The SHR algorithm exhibits high speed and does not require significant computing resources.

This study develops a general approach for analyzing HOS of oscillations, including non-pulse type, using fuzzy entropy (FuzzyEn) and SE calculations from the SHR time series. The major contributions of this study are as follows:

1. The method of entropy analysis of HOS is presented using the example of a digital-to-analog circuit of resistively coupled oscillators, including the effect of frequency-modulated noise. Using this method, entropy maps of the circuit synchronization states are constructed.

2. The dependence of FuzzyEn on the embedding vector length of the SHR time series is analyzed, based on which the synchronization states of the circuit are classified.

3. An algorithm for analyzing the HOS of non-pulse signals by the Hilbert transform is developed. As an example, experimental data (Scheffer-Teixeira and Tort, 2016) of the phase–phase coupling of θ- and γ-waves of local field potentials (LFPs) in the rat hippocampus are analyzed.

2 Methods

2.1 Workflow diagram of phase-locking entropy analysis

Fig. 1 shows the general workflow diagram of the proposed method for entropy analysis of phase-locking dynamics. At the first stage, it is necessary to construct pulse sequences (trains with the same pulse width) for the analyzed signals, which can be divided into two types: pulses and non-pulses. For pulse (relaxation) signals (denoted by blue squares), such as neuron spikes and electrocardiogram signals, rectangular trains are formed by a sharp change (rise or fall) in their amplitudes. If the signal is non-pulse, i.e., it is a smooth (non-relaxation) type (denoted by orange squares), it is necessary to first construct phase functions ($\varphi(t)$) with phase switching moments (for example, from π to $-\pi$) via the Hilbert transform and to associate rectangular pulses with them.

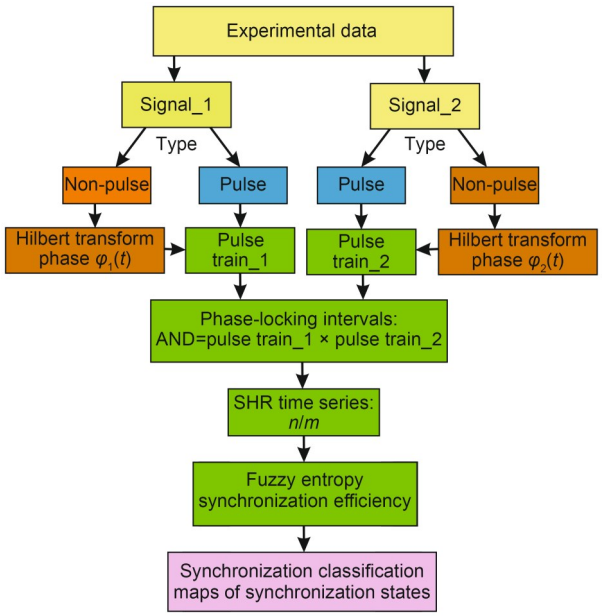

Fig. 1 Workflow diagram of phase-locking entropy analysis. References to color refer to the online version of this figure

FuzzyEn and SE are calculated for the SHR time series. At the final step, the HOS states of the system are classified based on their values. A synchronous state corresponds to a low FuzzyEn and high SE (~100%), whereas a non-synchronous state corresponds to a high FuzzyEn and low SE (<20%). The synchronization states are classified based on the dependence of FuzzyEn on the embedding vector length L of the SHR time series.

2.2 Circuit of resistively coupled pulse oscillators

In this study, the object of synchronization modeling is a digital–analog circuit of two resistively coupled pulse oscillators (Fig. 2a), with two resistors R_{12} and R_{21} placed between the inputs and outputs of the oscillators. Each oscillator is a simple self-oscillator based on two inverters with resistance–capacitance (RC) coupling (Fig. 2b). Because of the positive feedback between the input of the first (node 1) and the output of the second inverter (node 2) in the circuit (Fig. 2b), rectangular pulses are generated, with periods and durations proportional to the time constants $T_1=R_1\cdot C$ and $T_2=R_2\cdot C$, respectively. In this circuit, the gate diodes D_1 and D_2 allow independent adjustment of the pulse periods and widths by changing the resistances R_1 and R_2. The dynamics of a single-resistor

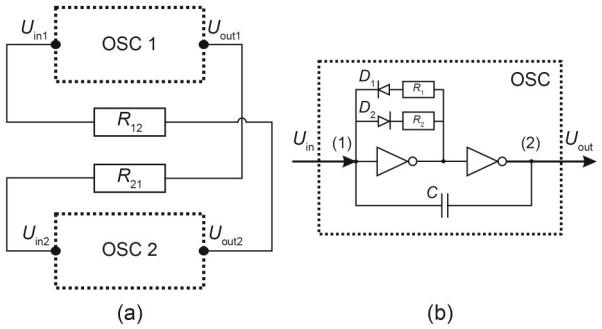

Fig. 2 Circuit of two resistively coupled pulse oscillators (OSC 1 and OSC 2) (a) and circuit of basic oscillator (OSC) with two NOT gates and RC coupling (b). The input (1) and output (2) nodes of the oscillator are indicated

circuit without diodes is described in Appendix A of Boriskov (2024).

The parameters of basic oscillator circuits (OSC 1 and OSC 2) used in all calculations are listed in Table 1. The NOT logic gate has a supply voltage U_s=5 V and low and high levels (U_{low}=1.5 V and U_{high}=3.5 V). These two oscillators have equal capacitance C and resistance R_2. Thus, the pulse widths are the same in the absence of resistive coupling. Furthermore, the intrinsic pulse periods of the oscillators, determined by resistances R_1, differ by more than twice (~2.3, Table 1). The oscillator with a shorter pulse period (higher frequency) is designated as the leading oscillator (OSC 1), whereas the oscillator with a lower frequency is designated as the lagging oscillator (OSC 2).

Although a full analysis of the dynamics of the circuit shown in Fig. 2a is beyond the scope of this study, the key aspects are important for subsequent analysis. The system of coupled oscillators outputs rectangular pulses OSC 1 and OSC 2 with controlled periods (frequencies) when resistance R_{12} or R_{21} is changed. The effect of one oscillator on the other oscillator manifests as additional currents at their inputs

Table 1 Parameters of basic oscillator circuits

Symbol and unit	OSC 1	OSC 2
C (nF)	100	100
R_1 (kΩ)	17	39
T_1 (ms)	1.7	3.9
R_2 (kΩ)	1	1
T_2 (ms)	0.1	0.1

Taken from Fig. 2b

(node 1) through these resistances, thereby reducing the frequency and the pulse rate. The lower the resistance (R_{12} or R_{21}), the greater the amplitude of the corresponding current (I_{12} or I_{21}), and the stronger the frequency suppression of the corresponding oscillator. The reverse effect of coupling currents on the oscillators through their outputs is absent, ensuring unidirectional current impact from the first oscillator to the second oscillator through R_{12}, and vice versa.

However, the pulse widths do not change significantly with the changes in R_{12} or R_{21}, which becomes more pronounced as the T_2/T_1 ratio decreases (no less than 17 times, Table 1). Thus, changing the coupling between oscillators through resistances R_{12} or R_{21} not only leads to different temporal correlations (synchronization) of the output pulses but also controls their frequency modulation.

2.3 HOS metrics of pulse oscillations

Phase synchronization is defined as the constancy of instantaneous phase relationships between signals, implying that no phase precession is present, and the phase of one signal always accurately predicts the phase of the other signal (Pikovsky et al., 2002). The mathematical condition for phase locking n:m of two signals with phases $\varphi_1(t)$ and $\varphi_2(t)$ is given by

$$\Delta\varphi_{nm}=\left|n\varphi_1(t)-m\varphi_2(t)\right|<\varepsilon \text{ for any } t, \tag{2}$$

where n and m are integers, and ε denotes a small number. Instantaneous phases of narrowband signals are determined based on analytical signals using the Hilbert transform (Rabiner et al., 1978). In general, for most signals, including relaxation (pulse) signals, the wrapped phase $\varphi(t)$ can be understood as a function proportional to the fraction of the period, increasing by 2π during one oscillation cycle (switching):

$$\varphi(t)=2\pi\frac{t-t_1}{t_2-t_1},\ t_1<t\le t_2, \tag{3}$$

where t_1 and t_2 denote the start and end times of one cycle respectively, which coincide with the neighboring pulse switching times (either the ON→OFF or OFF→ON time).

The effect of synchronization with different n and m values is also called subharmonic synchronization (or HOS) because the spectra of both periodic signals contain coinciding frequencies $m\omega_{01}=n\omega_{02}$, where ω_{01} and ω_{02} denote the fundamental spectral frequencies of the first and second signals, respectively. The n:m ratio is called SHR (Velichko et al., 2018b). This ratio is inversely proportional to the number of periods of each oscillator fitting into a certain interval. Fig. 3 shows an example of HOS synchronization with SHR=2:5 satisfying condition (2).

HOS can be identified without evaluating condition (2). With an initial zero phase shift, the pulses can be simply multiplied (Fig. 3a); i.e., they can be assigned a pulse train that represents a logical multiplication function (pulse 1 AND pulse 2). If this train is a periodic sequence of single pulses, the original pulse signals are synchronized and satisfy condition

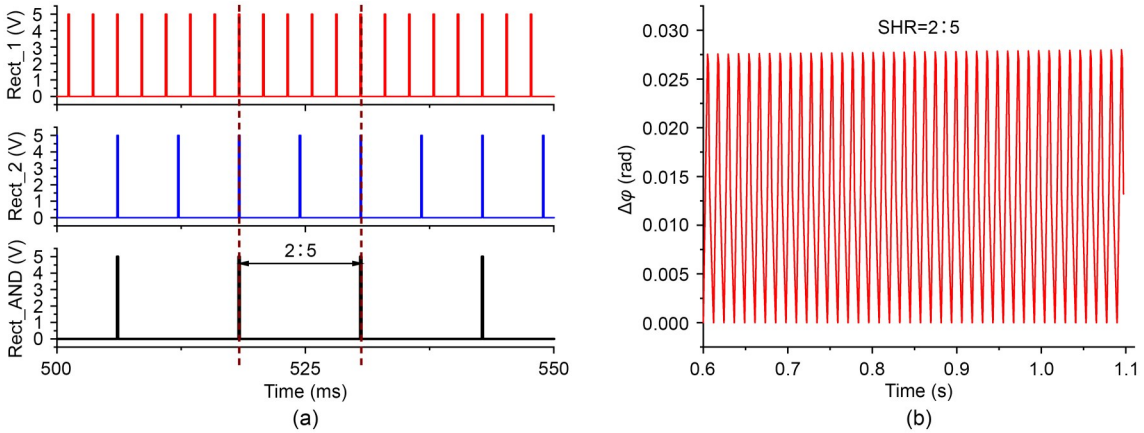

Fig. 3 Oscillograms of type 1 HOS with SHR=2:5 showing the output pulses of master (Rect_1) and slave (Rect_2) oscillators and their multiplication (Rect_AND) (a) and phase difference module Δφ with m=5 and n=2 of output voltages Rect_1 and Rect_2 (b). The calculation parameters are listed in Table 2. References to color refer to the online version of this figure

(2). In quasi-regular synchronization of two signals, different SHR values are observed in various phase-locking intervals, resulting in a time series of rational SHR values. Using the AND operation to assess the SHR values of two pulse sequences, we determine the coincidence positions and then count the number of periods of the first (n) and second (m) signals between them. By performing this procedure for each period of the multiplied pulse signal, a binary series consisting of pairs of n and m numbers is obtained. These pairs can also be assigned SHR values as rational fractions n/m. HOS can also be characterized by the SE metric, which is defined as the maximum probability $P_{\max}$ in the SHR distribution (Velichko et al., 2018a; Velichko, 2019):

$$\mathrm{SE}=P_{\max}(n_1{:}m_1)\times 100\%, \tag{4}$$

where $n_1{:}m_1$ denotes the ratio (not division) with the highest relative frequency in the SHR time series.

2.4 Fuzzy entropy and classification of synchronization states

In this study, we use FuzzyEn, a widely used metric in applied and theoretical entropy data analyses, to assess the regularity of time series (Ishikawa and Mieno, 1979; Chen et al., 2007). As shown in Boriskov et al. (2024), FuzzyEn is highly sensitive to changes in the degree of regularity of the SHR time series.

The principle of FuzzyEn calculation is based on the conditional probability that if vectors (segments of the time series) of length L are similar within an acceptable deviation, vectors of length L+1 will also be similar within the same deviation. For a time series of length N, $N-L$+1 vectors can be compared. The similarity metric (correlation) between vectors is a fuzzy function that calculates the distances between a pair of compared vectors:

$$D_{ij}^{L}=\exp\left(-\frac{\left(d_{ij}^{L}\right)^{r_2}}{r_1}\right), \tag{5}$$

where $d_{ij}^{L}=\max\limits_{k\in(0,L-1)}\left|\boldsymbol{x}_{i+k}-\boldsymbol{x}_{j+k}\right|$ denotes the Chebyshev distance between vectors, defined as the maximum difference between their components. Using fuzzy similarity, the probability of similar patterns of length L appearing in time series N is calculated as follows:

$$\phi^{L}(r_1,r_2)=\frac{1}{N-L}\sum_{i=1}^{N-L}\left(\frac{1}{N-L-1}\sum_{j=1,j\neq i}^{N-L}D_{ij}^{L}\right). \tag{6}$$

The numerator is the sum of similarity degrees for each pair of vectors. The final value of FuzzyEn is defined as the negative natural logarithm of the ratio of the sum of the similarity degrees of vectors of lengths L and L+1:

$$\mathrm{Fuzzy}(L,r_1,r_2)=\ln\left(\frac{\phi^{L}(r_1,r_2)}{\phi^{L+1}(r_1,r_2)}\right). \tag{7}$$

The primary adjustable parameters of FuzzyEn (7) are the embedding vector length L, inverse exponent r_1, and exponent r_2. The minimum dimension (length) of the vector L=1 is most frequently used as a standard parameter. The parameter r_1 defines the permissible deviation of elements and is taken within the range of 0.005std–0.4std, where std denotes the standard deviation of the series elements (by default r_1=0.01std). The power dependence exponent r_2 is by default equal to 1. The default values of r_1 and r_2 are used in all calculations in this study.

The FuzzyEn values of the SHR time series are analyzed to classify the synchronization states of the oscillator circuit. The analysis is focused on the dependence of FuzzyEn on the embedding vector length L. Low FuzzyEn values indicate high synchronization, whereas high FuzzyEn values indicate low synchronization. By studying the FuzzyEn values for different embedding vector lengths, the synchronization states of the oscillator circuit are classified into different categories, providing a detailed understanding of the synchronization dynamics.

3 Results

3.1 Variants of HOS in pulse oscillator circuit

Figs. 3–5 show various dynamic modes of the coupled oscillator circuits with different resistance R_{12} and R_{21} values (Table 2). Fig. 3 shows the complete HOS of the pulses from the two oscillators (type 1). The oscillogram of the pulse multiplication (bottom

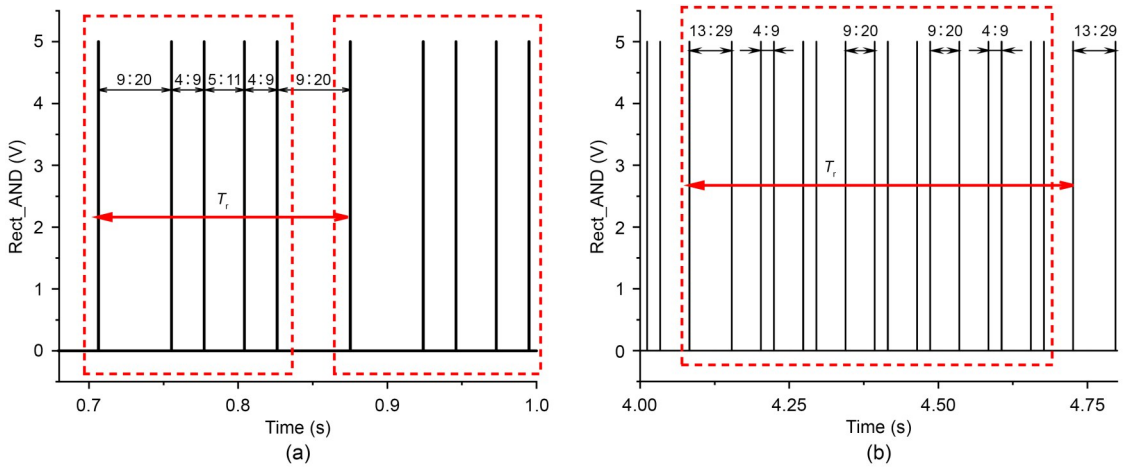

Fig. 4 Oscillograms of multiplication of oscillator output pulses (Rect_AND) for type 2 HOS: (a) type 2a; (b) type 2b. Groups of pulses with 5 (a) and 16 (b) periods, T_r (red arrows) with SHR sets (9:20, 4:9, 5:11) and (13:29, 9:20, 4:9), respectively, are indicated by red dashed rectangles. The calculation parameters are listed in Table 2. References to color refer to the online version of this figure

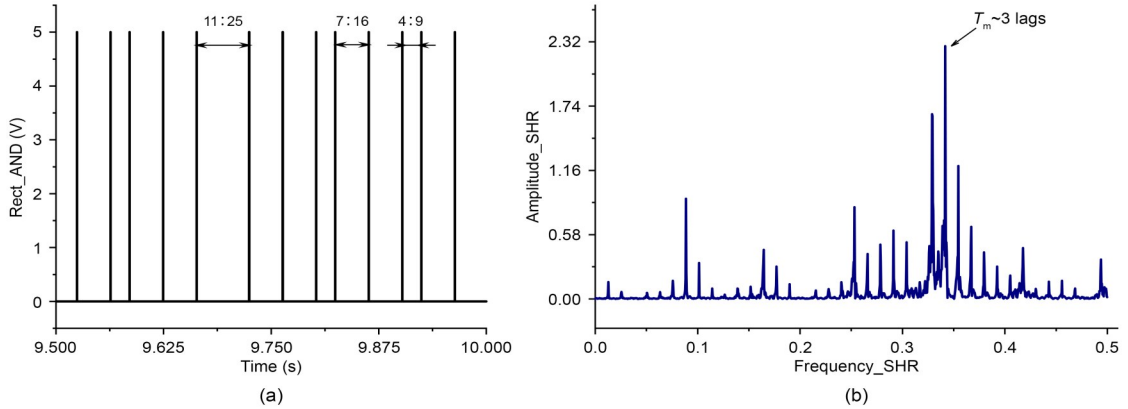

Fig. 5 Oscillogram of multiplication of oscillator output pulses (Rect_AND) (a) and AFR of SHR time series (b) for type 3 HOS. AFR is a one-sided spectrum of SHR series (n/m, minus the constant component) calculated for the number of samples N=3000 and a time step (lag) equal to one. The values from the set (11:25, 7:16, 4:9) of the SHR series and its period T_m with the maximum amplitude of the spectrum are shown. The calculation parameters are listed in Table 2

Table 2 Parameters of coupling resistances of the circuit shown in Fig. 2a for three HOS types

Synchronization type	Figure	R_{12} (MΩ)	R_{21} (MΩ)
Regular HOS (type 1)	Fig. 3	1.1	0.4
Regular chimeric HOS (type 2: 2a and 2b)	Fig. 4a	1.1	1.7
	Fig. 4b	1.1	1.6
Quasi-regular chimeric HOS (type 3)	Fig. 5	1.4	0.9

The oscillator parameters are listed in Table 1

of Fig. 3a) is a strictly regular sequence of single pulses, in which there are five and two periods of OSC 1 and OSC 2 pulses, respectively, i.e., SHR= 2:5. As shown in Fig. 3b, condition (2) for the modulus of the phase difference $\Delta\varphi_{nm}$ with m=5 and n=2 calculated using Eq. (3) is satisfied for values of ε not exceeding 0.03 rad.

Fig. 4 presents examples of the second type of HOS dynamics (type 2) in two variants (2a and 2b), where the product of oscillator pulses forms periodic

sequences grouped into batches of 5 pulses (Fig. 4a, type 2a) and 16 pulses (Fig. 4b, type 2b). In this case, the rows also represent periodic sets (with periods of 5 and 16) of the SHR ratios 9:20, 4:9, 5:11 and 13:29, 9:20, 4:9 for variants 2a and 2b, respectively. For example, in variant 2a (Fig. 4a), the SHR sequence (9:20, 4:9, 5:11, 4:9, 9:20) has repeating sequences.

The oscillograms in Fig. 5a show the third type of circuit dynamics, where the output pulses of the oscillators form a quasi-periodic sequence of multiplication pulses. Unlike type 2 HOS, this type has a quasi-periodic set of three SHR ratios: 11:25, 4:9, and 7:16. If these three ratios are denoted with letters *a*, *b*, and *c*, separately, the SHR sequence can be represented as (⋯, *c*, *b*, *c*, *c*, *b*, *c*, *c*, *b*, *c*, *a*, *c*, *b*, *c*, *c*, *b*, *c*, *a*, *c*, *b*, *c*, *c*, *b*, *c*, *a*, *c*, *b*, *c*, *b*, *c*, *c*, *b*, *c*, *c*, *b*, *c*, *c*, *b*, *c*, *a*, *c*, *b*, *c*, *c*, *b*, *c*, *a*, ⋯). In HOS type 3, the values repeat only within short intervals, and the regularity of the series is disrupted because SHR=11:25 (letter *a*) is inserted in random positions. The amplitude–frequency response (AFR) of SHR (Fig.5b) shows the most frequent repetition interval T_m, consisting of the sequence (7:16, 4:9, 7:16), i.e., (*c*, *b*, *c*).

The SE for three types of oscillator circuit dynamics is calculated. For complete HOS (type 1, Fig. 3), SE=100%. For type 2, SE=40% (Fig. 4a) and 56% (Fig. 4b), with the most frequent value being SHR=9:20. In the case of quasi-periodic synchronization of type 3 (Fig. 5), the most frequent value, SHR=7:16, has SE=66%. If the first type of dynamics with SE=100% representing true HOS according to condition (2), the second and third types, where this condition is not met, can be called regular and quasi-regular chimeric HOS, respectively.

Thus, the dynamics of the coupled pulse oscillators (Fig. 2) is classified into three types, among which the real HOS is the first variant (Fig. 3). Strong coupling between oscillators ensures their synchronous interaction and fulfillment of condition (2) only in this case. The dynamics of regular chimeric HOS types 2a and 2b (Fig. 4) is initiated by very weak interactions between the oscillators with periodic pulse period variations and SHR series. This synchronization is analogous to a time-varying phase shift of two independent signals with commensurate frequencies. Quasi-regular chimeric HOS (type 3, Fig. 5) results from weak interactions between oscillators, initiating fluctuations in pulse periods with disturbances in the periodicity of the SHR series. For HOS types 2 and 3, the phase difference of the pulses grows indefinitely for any *n* and *m*; i.e., condition (2) is not met.

Fig. 6 shows the dependence of FuzzyEn on the embedding vector length *L* for the three HOS types presented in Figs. 3–5. The complete HOS with SE=100% (Fig. 3) is expected to have zero entropy at any *L* (black curve (1), Fig. 6). In the case of the regular chimera HOS (type 2), FuzzyEn is high at *L*=1 and only reaches zero as *L* increases. The synchronization entropy of type 2a (Fig. 4a) is zero at the second step of *L* (Fig. 6, red curve (2a)), whereas that of type 2b (Fig. 4b) drops to zero only at *L*=11 (Fig. 6, blue curve (2b)). This is due to the distinct periodicity of chimera synchronization: In the second variant, the SHR series has a significantly longer period and greater variations in value. However, the periods (5 and 16) of these regular types of HOS do not match the values of *L* at which FuzzyEn becomes zero (2 and 11, respectively).

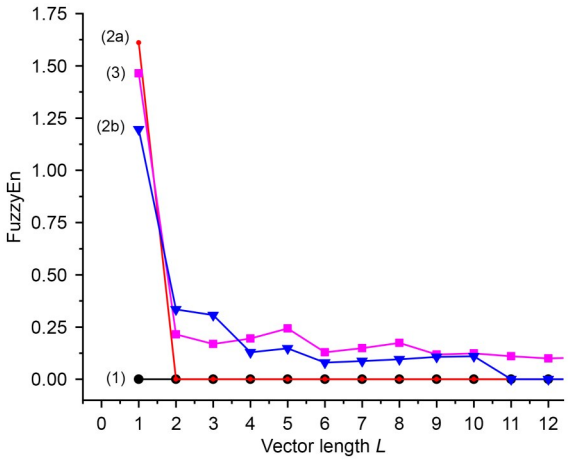

Fig. 6 Dependencies of FuzzyEn on embedding vector length *L* of SHR series for three HOS types. The black (1), red (2a) and blue (2b), and magenta (3) curves indicate type 1, type 2, and type 3, respectively. References to color refer to the online version of this figure

In the case of quasi-periodic chimera HOS (type 3, Fig. 5), FuzzyEn does not drop to zero with increasing embedding vector length but instead reaches a constant value (Fig. 6, magenta curve (3)). Thus, by changing *L*, one can adjust the sensitivity of the FuzzyEn method to detect synchronization states.

3.2 Distribution maps of HOS states in pulse oscillator circuit

In the oscillator circuit shown in Fig. 2a, for each pair of resistances R_{12} and R_{21} in the range of 0.2–2.1 MΩ with a step of 100 kΩ, the SHR time series is calculated to determine the degree of synchronization.

3.2.1 SE map

Fig. 7 shows the SE distribution map, indicating constant SHR values at 100% efficiency. In the left part of the map (small R_{21} values), an HOS area with an SHR ratio of 1∶3 is observed. This area corresponds to the significant influence of the slow (follower) oscillator OSC 2 on the fast (leader) oscillator OSC 1 through a small R_{21} value less than 0.3 MΩ.

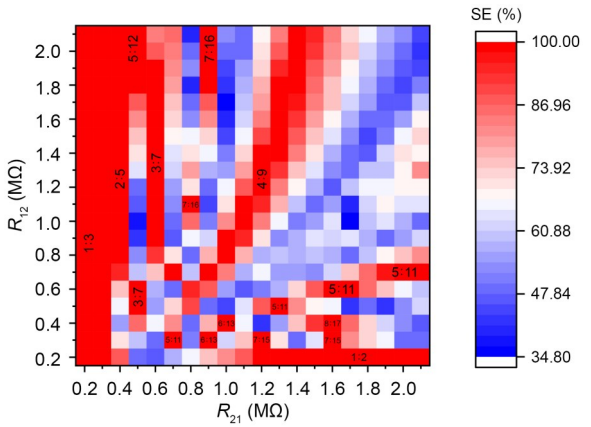

Fig. 7 SE distribution map. SHR values in areas with SE=100% are indicated. The basic oscillator parameters (Fig. 2b) are listed in Table 1. References to color refer to the online version of this figure

The influence of the follower oscillator decreases (the current I_{21} drops) as the resistance R_{21} increases, and high-HOS areas with SHR=2:5 are observed on the map. Further to the right edge of the map, synchronization zones with other SHR values (3:7, 7:16, 4:9, etc.) are visible, where the SHR value gradually approaches the ratio of the natural frequencies of the oscillators (n/m≈0.4545). The largest HOS area corresponding to SHR=4:9 is located near the diagonal of the map, where the frequency of the fast oscillator differs from the free oscillation frequency by less than 2%. Next to the SHR=4:9 area, there is a diagonal zone with low SE, which divides the map into two parts, as indicated by the blue and white–blue colors in Fig. 7. Below and to the left of this diagonal, small zones in which the n/m value exceeds 0.452 are observed, with SHR=5:11, 6:13, 7:15, and 8:17. In these areas, the frequency of the follower oscillator begins to adjust to the frequency of the leader oscillator, reducing the oscillation period until the nearest SHR value of 1:2 is reached.

3.2.2 FuzzyEn distribution map of SHR series

Fig. 8 shows the FuzzyEn distribution maps of the SHR time series for embedding vector length L=1–4. On the map with L=1, entropy exhibits a pronounced negative correlation with SE (Fig. 7); i.e., in areas in which SE approaches 100%, FuzzyEn approaches zero, and vice versa. The average Pearson correlation coefficient calculated from the SE and FuzzyEn distribution maps with L=1 is −0.903, indicating a high negative correlation between entropy and SE.

There are visible blue areas on the maps (Fig. 8) where FuzzyEn is close to zero, consistent with SE=100% (red area, Fig. 7). As the vector length L increases from 2 to 4, the maps show a decrease in entropy and an increase in blue areas; thus, at L=4, only isolated red areas of high FuzzyEn remain (Fig. 8d). Increasing the length of the embedding vector L allows the most unsynchronized areas of dynamics to be highlighted on the map and provides additional information about the areas of partial (quasi-periodic) HOS of oscillators.

3.3 HOS in pulse oscillator circuit under noise influence

To investigate the effect of HOS under white noise, we introduce noise that exclusively affects the frequency modulation of oscillators, causing fluctuations in pulse periods relative to their average values. The circuit (Fig. 2a) comprises two independent white noise generators, each of which randomly varies the resistance R_1 of its oscillator (Fig. 2b) and the time constants $T_1=R_1\cdot C$, which determine the pulse periods. The Simulink circuit (Fig. 2a) of each basic oscillator (OSC 1 and OSC 2) includes a variable resistance module, previously developed by our team, as shown in Appendix B of Boriskov (2024), controlled by a noise signal $U_n(t)$ according to the linear law.

$$R_1(t)=R_o+K_n\cdot U_n(t), \tag{8}$$

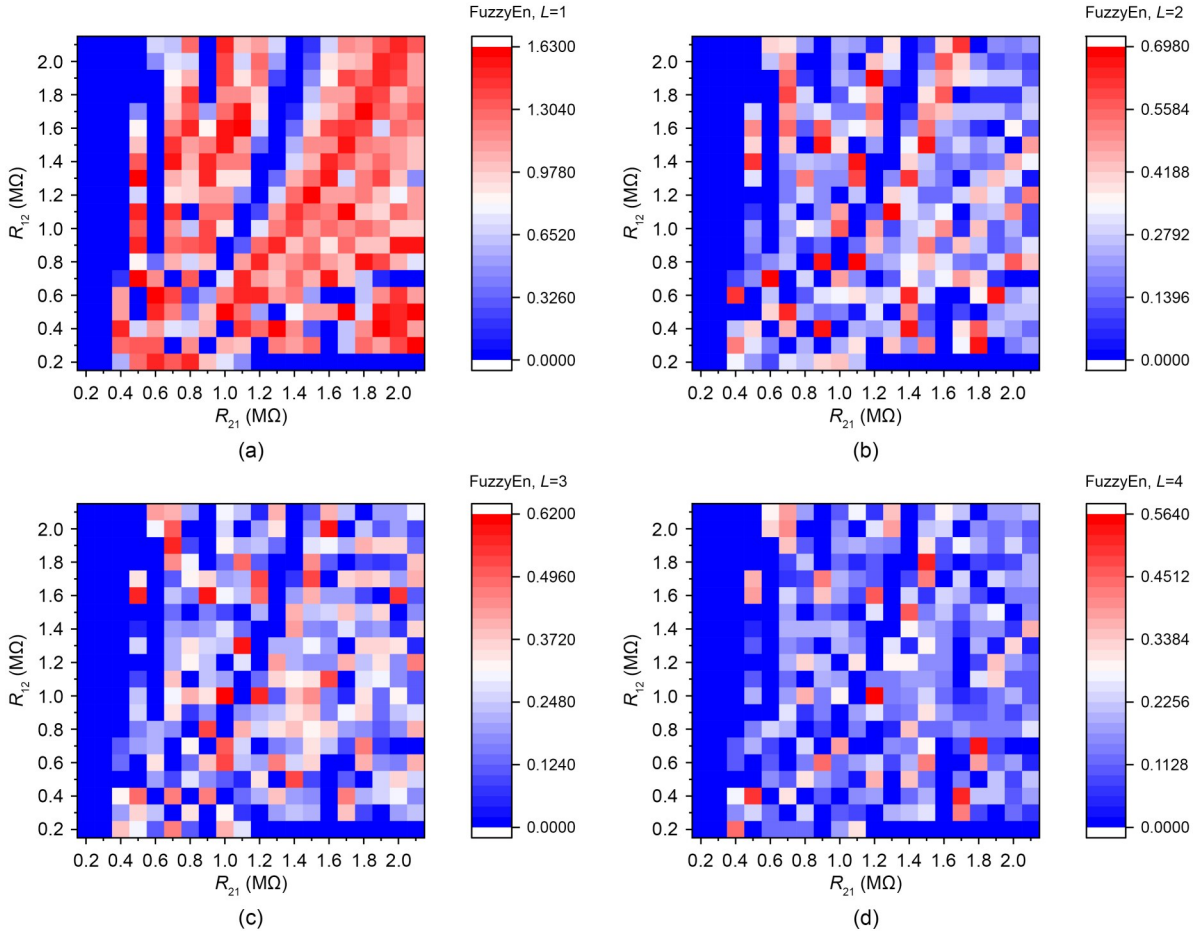

Fig. 8 FuzzyEn distribution maps for embedding vector lengths of SHR series: (a) L=1; (b) L=2; (c) L=3; (d) L=4. The basic oscillator parameters (Fig. 2b) are listed in Table 1. References to color refer to the online version of this figure

where R_o denotes the reference resistance, and K_n denotes the white noise gain coefficient. The discrete white noise $U_n(t)$ has standard parameters with a mean of zero and power P_n determined from the variance D_n and sampling step t_n.

$$P_n=\sqrt{D_n\cdot t_n}. \tag{9}$$

The noise sampling step in the simulation is selected as t_n=0.01 s, which is approximately half the average pulse period of the master oscillator. The case of identical noise generators affecting the basic oscillators is analyzed. The parameters of the basic oscillator (Fig. 2b) are presented in Table 1, with the exception of the resistance R_1, which now randomly varies over time according to Eq. (8). In turn, the reference resistance R_o in Eq. (8) for both oscillators OSC 1 and OSC 2 are equal to the former constant values of R_1 from Table 1.

Fig. 9 shows the SE and FuzzyEn distribution maps for an embedding vector length L=1 under the influence of white noise. As expected, these maps are also inverse to each other but become blurred compared with the synchronization state maps without noise (comparison of Figs. 7 and 8a).

The highly synchronized states of the oscillator circuit under noise are maintained only at the left edges of the maps and have maximum SE values of approximately 80% (red color in Fig. 9a) and minimum FuzzyEn values of approximately 0.62 (blue color in Fig. 9b). These values approximately correspond to the average SE (white–red color in Fig. 7) and FuzzyEn (white–blue color in Fig. 8a) in the noise-free oscillator circuit.

Fig. 10 shows an example of HOS fluctuations in the SHR series under a noise power of P_n=24 mW. The level of SHR=1∶3 is visible, corresponding to full HOS in the absence of noise. Fig. 10b shows the

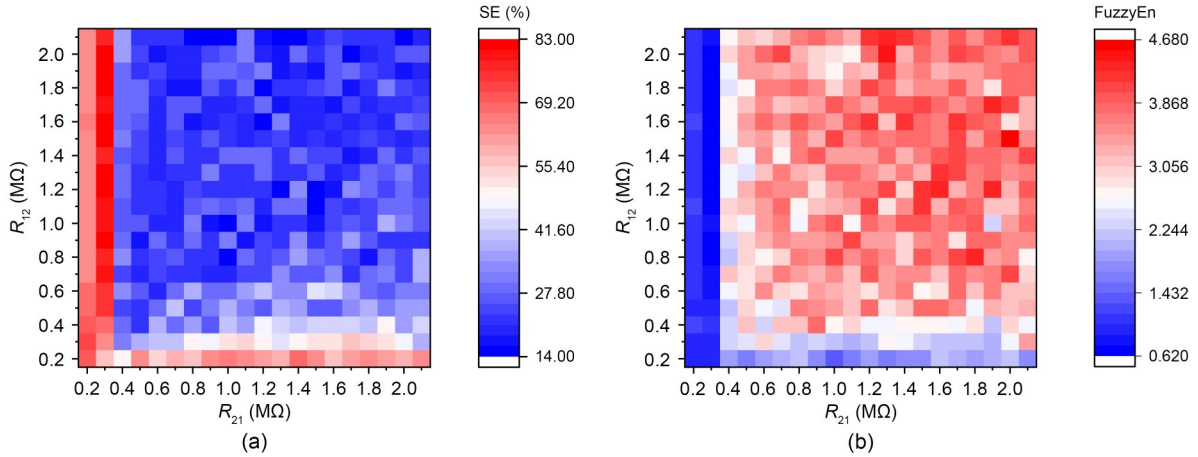

Fig. 9 Distribution maps of SE (a) and FuzzyEn (b) under the influence of noise. The calculation parameters are K_n= 10 kΩ/W and P_n=24 mW. References to color refer to the online version of this figure

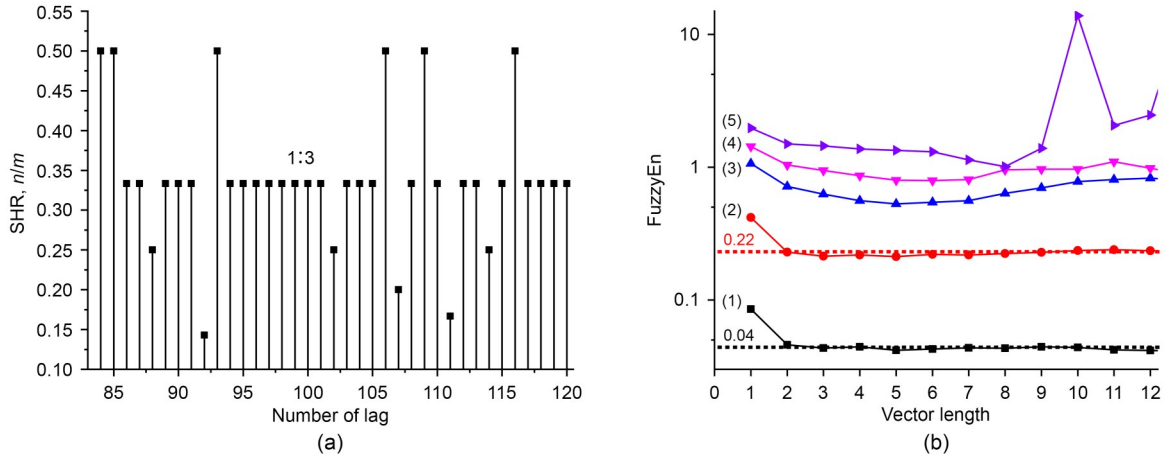

Fig. 10 (a) SHR time series (ratios n/m) under noise power P_n=24 mW. (b) Dependencies of FuzzyEn (logarithmic scale) on the embedding vector length L for increasing noise power: curve (1) with P_n =10 mW, curve (2) with P_n =14 mW, curve (3) with P_n =24 mW, curve (4) with P_n =27 mW, and curve (5) with P_n =45 mW. The other calculation parameters are R_{12}=1.2 MΩ, R_{21}=0.2 MΩ, K_n=10 kΩ/W. SHR values at the level of 0.333 (1:3) are marked in Fig. 10a. The steady-state levels of FuzzyEn for curves (1) and (2) are shown in Fig. 10b. References to color refer to the online version of this figure

FuzzyEn dependencies on the embedding vector length L for different noise power levels. For the smallest noise powers (curves (1) and (2)), FuzzyEn reaches a steady low level for L>1. As the noise power increases, the entropy increases and begins to oscillate weakly around the mean level, which does not decrease with increasing L (curves (3) and (4)). At the highest noise levels, FuzzyEn oscillations become unstable, with a sharp increase when L reaches larger values (curve (5), L=10).

Noise affects the dynamics of the oscillators, resulting in HOS failures and a gradual increase in FuzzyEn with increasing noise power. For the smallest noise powers (curves (1) and (2), Fig. 10b), the FuzzyEn dependencies on L resemble curves (2a) and (2b) in Fig. 6, indicating HOS type 2. As noise power increases, HOS failures increase, and the regularity of the SHR series decreases. In this case, with increasing L, entropy begins to oscillate slightly but does not fall to a low level (curves (3) and (4), Fig. 10b), resembling quasi-regular HOS type 3 (blue curve (3), Fig. 6). The highest noise power initiates the destruction of the HOS of the oscillators. Significant fluctuations in the SHR series lead to entropy calculation instability (curves (5)–(7)): with increasing L, the amplitude of FuzzyEn oscillations increases (curve (5), Fig. 10b). Such a self-excitation mode is a characteristic of FuzzyEn for any highly irregular (chaotic) signal.

Thus, entropy instability with increasing embedding vector length indicates strong chaos in the SHR time series and loss of synchronization in the circuit under sufficiently high noise power.

3.4 Entropy analysis of HOS for non-pulse signals

In Section 3.3, the synchronization of pulse (non-smooth) signals generated by the model circuit (Fig. 2) was analyzed. In this subsection, the entropy analysis method is extended to non-pulse (non-spike) signals, which are defined by continuous derivatives at all time points and a limited spectral width. In this regard, we transform smooth (differentiable) signals into analytical signals using the Hilbert transform (Rabiner et al., 1978). From the analytical signals, we extract phase functions of the wrapped type, i.e., instantaneous phases $\phi_1(t)$ and $\phi_2(t)$, representing rotation angles in the range $[-\pi, \pi]$. To the phase switching moments from π to $-\pi$, we assign rectangular pulses of short duration relative to the average pulse periods (Fig. 1). Thus, for the initial non-pulse signals, two pulse trains are formed based on the phases $\phi_1(t)$ and $\phi_2(t)$. Next, the SHR series is calculated for these pulse trains using the AND operation, and the synchronization indicators SE and FuzzyEn are evaluated.

As an example, we consider the experimental LFP data of the rat hippocampus from the database (Scheffer-Teixeira and Tort, 2016). LFP brain activity signals can include several rhythms: θ (4–8 Hz), α (8–14 Hz), β (14–30 Hz), and γ (30–150 Hz). The gamma rhythm is further divided into three subranges, namely, γ_s, γ_m, and γ_f, with γ_s being the most significant in the 30–50-Hz range. Many studies have hypothesized that phase–phase coupling between θ and γ_s rhythms of the hippocampus indicates synchronized activity of individual hippocampal neurons (Belluscio et al., 2012; Xu et al., 2013; Zheng et al., 2016). However, this view has been challenged primarily on technical grounds (Scheffer-Teixeira and Tort, 2016). The θ and γ_s oscillations are extracted from the LFP signal by passing it through a digital Butterworth bandpass filter in the θ- and γ_s-rhythm ranges. The advantage of the Butterworth filter is its uniform AFR within the passband. To ensure a sharp roll-off at the band edges, the highest possible filter order is used (up to the self-oscillation mode), which is 4 and 7 for the θ- and γ_s-rhythm ranges, respectively. In addition, the well-known method of double (forward and backward) passage of the LFP signal through the filter is applied to suppress nonlinear phase distortions.

The Hilbert transform is applied to the obtained θ- and γ_s-oscillations to yield phase functions (θ and γ_s phases) and pulse trains (θ and γ_s pulses) using the aforementioned algorithm, as demonstrated by the example in Fig. 11. Finally, the SHR time series are calculated for the θ and γ_s pulses, and the SE value and the FuzzyEn function of the embedding vector lengths L are estimated.

Fig. 12a shows the dependencies of FuzzyEn on the embedding vector length L for the LFP θ and γ_s signals (from six rats) randomly selected from the database in Scheffer-Teixeira and Tort (2016). The entropy curves are split into two groups. In the first group (curves (1)–(3)), entropy decreases to zero as L increases, indicating an analogy with HOS type 2 (compared with curve (2b) in Fig. 6) and some connection between the θ and γ_s rhythms. The second group of FuzzyEn curves (4)–(6) indicates the presence of strong noise in the LFP signals, because entropy exhibits a large oscillation amplitude and remains at a high level. LFP noise may be due to technical reasons (e.g., LFP registration noise) or other factors, such as the brain activity of animals (e.g., fluctuations in excitation and rest intervals). Because the first group reveals rhythm synchronization, we hypothesize that the entropy curves (4)–(6) are simply unsuccessful LFP signal registrations with a strong noise background. This hypothesis is also supported by the SE assessments shown in Fig. 12b. The maximum relative frequencies in the distributions are found for SHR=1:7 in all six datasets, whereas SE values are significantly lower for heavily noise-contaminated LFP signals (curves (4)–(6), Fig. 12a).

This tendency for FuzzyEn to split into these two groups is also observed in other LFP datasets from the database in Scheffer-Teixeira and Tort (2016), with a predominance of entropy dependencies from the second group, indicating a strong noise component in the LFP signals. Therefore, analysis of HOS in LFP suggests a weak connection between θ and γ_s rhythms, indicating that their synchronization is limited. However, because brain activity and the network system inherently operate within a stochastic

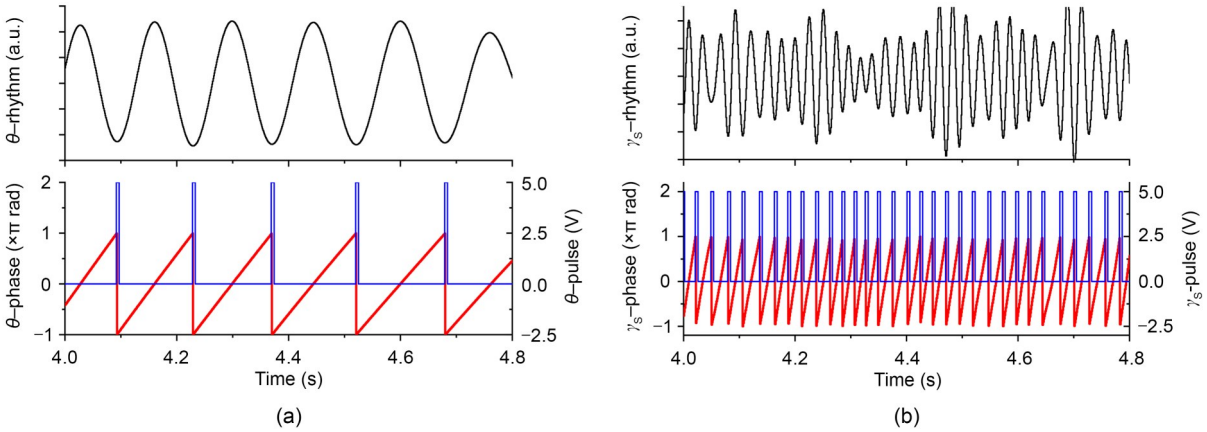

Fig. 11 LFP oscillograms (black curves) in a.u. (arbitrary units), phases (red curves), and pulse trains (blue curves) of θ (a) and γ_S (b) rhythms. Experimental LFP of the rat hippocampus is from a previous study (Scheffer-Teixeira and Tort, 2016). References to color refer to the online version of this figure

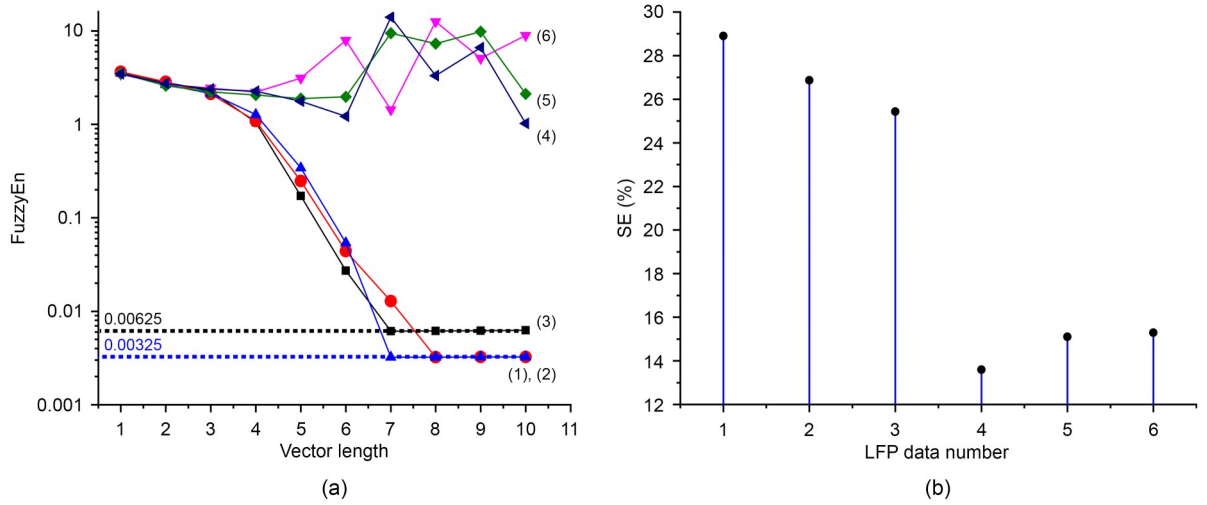

Fig. 12 Dependencies of FuzzyEn on embedding vector length L (a) and the SE value (b) of SHR time series of θ and γ_S rhythms for 6 rats (LFP data: (1)–(6)). The steady-state levels of FuzzyEn for curves (1), (2), and (3) are shown in Fig. 12a

framework, LFP data require more precise recording and processing, including statistical analysis, and larger recording and sample sizes. Although the analysis of neurophysiological data presented in this section is only "proof of principle," the new approach can yield interesting results and be used to evaluate phase-locking dynamics.

4 Discussion

This section summarizes the proposed method (Fig. 1). To analyze the synchronization type and degree of signals obtained from experimental data, sequences of rectangular pulses are formed. The signals can be of any (pulse or non-pulse) type. For pulse or spiking signals (denoted by blue squares in Fig. 1), pulses of constant duration are generated during switching or sharp transitions, such as from low to high values. For smooth (differentiable) signals, such as narrowband signals, pulse trains are formed by switching phase functions calculated from analytical signals using the Hilbert transform (denoted by orange squares, Fig. 1).

Alternative methods for forming pulse trains from non-pulse signals can also be considered. For example, a simple method involves generating pulses at the moments of maximum values (peaks) of oscillating

signals. However, it is necessary to monitor false peaks initiated by noise, which can significantly distort the phase-locking dynamics of the system under study. The resulting pulse trains must have coinciding pulses for some (initial) time instant, i.e., zero phase shift. Otherwise, the pulse trains may be synchronized but have zero multiplication. This occurs, for example, when the signals exhibit a shift greater than the pulse width.

Next, using the AND procedure, the SHR time series in the form of rational fractions of pulse periods n/m are formed, and SE and FuzzyEn are calculated. The ultimate goal of entropy analysis can be a simple classification of phase locking n:m, i.e., determining whether HOS exists, which is decided by assessing SE or FuzzyEn with L=1, for example, by some threshold value.

In addition, SE and FuzzyEn can be used to create maps of the HOS states of the analyzed systems controlled by a set of parameters. A more complex assessment of the degree and type of synchronization is performed with increasing lengths of embedding vectors of the SHR series. For example, by increasing the vector length, the most unsynchronized areas of the system dynamics can be highlighted on FuzzyEn maps.

The proposed approach uses the structure of the SHR time series to calculate entropy, which forms the basis for conclusions about system synchronization. In the case of partial (chimeric) HOS (Figs. 4 and 5) or under the influence of moderate noise (curves (2)–(4), Fig. 10b), the ratios of oscillator periods fluctuate around average values with small dispersion. For example, the relative standard deviation of the n/m ratios in the SHR series (Fig. 4a) does not exceed 1.2%. Three pairs of periods from the set (9:20, 4:9, 5:11) differ significantly from each other. In Fig. 4, a significant difference in periods is observed in the oscillograms of the multiplication (Rect_AND) of the output pulses of the oscillators. Even small fluctuations in the frequency of oscillators lead to a significant spread of distances between the moments of pulse coincidences. Consequently, a significant difference is observed in the integer SHR pairs at different time intervals, i.e., the multiplication signal periods.

The SHR time series most adequately reflects the dynamics of synchronization. A time series composed of pulse periods of the multiplication (AND) signal can also be used for entropy analysis of HOS. The disadvantage of this method is that the ratio of periods strongly depends on the frequency (period) fluctuations of pulse signals. Even under weak noise impact, high dispersion and entropy are observed. In this case, the synchronization pattern is heavily noisy, which complicates the analysis. The use of the ratio of the number of periods instead of the period values in the SHR series is analogous to filtering, where frequency fluctuations are averaged. More detailed analysis of this issue should be performed in future studies.

The self-excitation mode of FuzzyEn, where oscillations of high amplitude appear with increasing embedding vector length, is due to the loss of algorithm stability (Eqs. (5)–(7)) for finite irregular time series. With a sufficiently long embedding vector L, no similar patterns of length L+1 may be encountered. However, because fuzzy similarity (Eq. (5)) is used in the FuzzyEn calculation, the probability for patterns of length L+1 may be minimal but not zero. Consequently, the ratio of probabilities for patterns of lengths L and L+1 can suddenly increase for certain values, thereby increasing FuzzyEn. Thus, the self-excitation of FuzzyEn is caused by the loss of statistical stability of the calculation as L increases for a highly noisy (chaotic) finite series. This instability can only be overcome by increasing the length N of the series to a size where the probability of finding similar long patterns becomes statistically significant. For a regular (or nearly regular) finite series, the self-excitation of the algorithm cannot occur as long as $L<N$ and FuzzyEn approaches zero with increasing L, because the probabilities of finding similar patterns of lengths L and L+1 become identical.

This study demonstrates that the dependence of FuzzyEn on the embedding vector length L provides valuable information about the synchronization dynamics in the system. The loss of FuzzyEn stability with increasing L indicates chaotic dynamics in the SHR series and a lack of synchronization. Conversely, stable FuzzyEn behavior indicates regularity and predictability of the time-series dynamics, with the system in a synchronized state. In addition, a decrease in FuzzyEn

with increasing L suggests that the series contains hidden regularity, which becomes more pronounced at higher embedding vector dimensions.

Notably, synchronization detection for non-pulse signals requires an additional calculation of the phase functions of the signals using the Hilbert transform. However, this transform has technical solutions for digital platforms using discrete Hilbert filters (Schüßler and Steffen, 1998).

5 Conclusions

The proposed approach for assessing HOS signals is useful in various science and technology domains, such as the evaluation and analysis of the synchronization of financial, meteorological, and physiological data, including biomedical diagnostics, and industrial equipment, such as electric motors and gearboxes. Its primary advantage over other methods is its ease of obtaining synchronization characteristics in the form of fractional–rational SHR sequences, which can be interactively obtained. Furthermore, the digital signals (rectangular waves) used in the proposed method make it promising for implementation in fully digital platforms, such as field-programmable gate array-based systems. Future research should aim to enhance the sensitivity of the proposed method to minor changes in synchronized signal dynamics, potentially using other entropy indicators and machine learning algorithms.

Contributors

Petr BORISKOV designed the research. Petr BORISKOV and Vadim PUTROLAYNEN processed the data and drafted the paper. Andrei VELICHKO and Kristina PELTONEN helped organize the paper. Petr BORISKOV, Andrei VELICHKO, and Kristina PELTONEN revised and finalized the paper.

Conflict of interest

All the authors declare that they have no conflict of interest.

Data availability

The data that support the findings of this study are available from the corresponding author upon reasonable request.

References

Alter O, Brown PO, Botstein D, 2000. Singular value decomposition for genome-wide expression data processing and modeling. *Proc Natl Acad Sci USA*, 97(18):10101-10106. https://doi.org/10.1073/pnas.97.18.10101

Belluscio MA, Mizuseki K, Schmidt R, et al., 2012. Cross-frequency phase-phase coupling between theta and gamma oscillations in the hippocampus. *J Neurosci*, 32(2):423-435. https://doi.org/10.1523/JNEUROSCI.4122-11.2012

Biagi PF, Piccolo R, Ermini A, et al., 2001. Possible earthquake precursors revealed by LF radio signals. *Nat Haz Earth Syst Sci*, 1(1-2):99-104. https://doi.org/10.5194/nhess-1-99-2001

Bonet-Jara J, Quijano-Lopez A, Morinigo-Sotelo D, et al., 2021. Sensorless speed estimation for the diagnosis of induction motors via MCSA. Review and commercial devices analysis. *Sensors*, 21(15):5037. https://doi.org/10.3390/s21155037

Boriskov P, 2024. Chaotic discrete map of pulse oscillator dynamics with threshold nonlinear rate coding. *Nonl Dyn*, 112(5):3917-3933. https://doi.org/10.1007/s11071-023-09217-9

Boriskov P, Putrolaynen V, Velichko A, et al., 2024. Entropy-based detection of synchronization of pulse oscillators: a comparative analysis of entropic measures. Proc SPIE 13217, 3rd Int Conf on Digital Technologies, Optics, and Materials Science, Article 132170Y. https://doi.org/10.1117/12.3036692

Chen WT, Wang ZZ, Xie HB, et al., 2007. Characterization of surface EMG signal based on fuzzy entropy. *IEEE Trans Neur Syst Rehabil Eng*, 15(2):266-272. https://doi.org/10.1109/TNSRE.2007.897025

Chou J, Bramhavar S, Ghosh S, et al., 2019. Analog coupled oscillator based weighted Ising machine. *Sci Rep*, 9(1): 14786. https://doi.org/10.1038/s41598-019-49699-5

Cui LL, Wang HB, Zhao DZ, et al., 2024. Synchronous odd symmetric transform for rolling bearing fault diagnosis. *Measurement*, 226:114184. https://doi.org/10.1016/j.measurement.2024.114184

Delgado-Bonal A, Marshak A, 2019. Approximate entropy and sample entropy: a comprehensive tutorial. *Entropy*, 21(6): 541. https://doi.org/10.3390/e21060541

Ishikawa A, Mieno H, 1979. The fuzzy entropy concept and its application. *Fuzzy Sets Syst*, 2(2):113-123. https://doi.org/10.1016/0165-0114(79)90020-4

Li H, Zhang CC, Zhang Y, et al., 2023. A fractional-N frequency synthesizer with phase synchronization and programmable phase control capability. *Microelectron J*, 142:105996. https://doi.org/10.1016/j.mejo.2023.105996

Lowet E, Roberts MJ, Bonizzi P, et al., 2016. Quantifying neural oscillatory synchronization: a comparison between spectral coherence and phase-locking value approaches. *PLoS ONE*, 11(1):e0146443. https://doi.org/10.1371/journal.pone.0146443

Mallick A, Bashar MK, Truesdell DS, et al., 2020. Using synchronized oscillators to compute the maximum independent set. *Nat Commun*, 11(1):4689. https://doi.org/10.1038/s41467-020-18445-1

Nikonov DE, Csaba G, Porod W, et al., 2015. Coupled-oscillator associative memory array operation for pattern recognition. *IEEE J Explor Sol State Comput Dev Circ*, 1:85-93.

https://doi.org/10.1109/JXCDC.2015.2504049

Park J, Mackay S, Wright E, 2003. Preface. In: Park J, Mackay S, Wright E (Eds.), Practical Data Communications for Instrumentation and Control. Newnes, Oxford, p.xi-xiii. https://doi.org/10.1016/B978-075065797-6/50000-9

Pikovsky A, Rosenblum M, Kurths J, et al., 2002. Synchronization: a universal concept in nonlinear science. *Am J Phys*, 70(6):655. https://doi.org/10.1119/1.1475332

Rabiner LR, Gold B, Yuen CK, 1978. Theory and application of digital signal processing. *IEEE Trans Syst Man Cybern*, 8(2):146. https://doi.org/10.1109/TSMC.1978.4309918

Ramírez E, Ruipérez-Campillo S, Castells F, et al., 2024. Novel synchronization method for vectorcardiogram reconstruction from ECG printouts: a comprehensive validation approach. *Biomed Signal Process Contr*, 91:106027. https://doi.org/10.1016/j.bspc.2024.106027

Romera M, Talatchian P, Tsunegi S, et al., 2018. Vowel recognition with four coupled spin-torque nano-oscillators. *Nature*, 563(7730):230-234. https://doi.org/10.1038/s41586-018-0632-y

Scheffer-Teixeira R, Tort ABL, 2016. On cross-frequency phase-phase coupling between theta and gamma oscillations in the hippocampus. *eLife*, 5:e20515. https://doi.org/10.7554/eLife.20515

Schüßler HW, Steffen P, 1998. Halfband filters and Hilbert transformers. *Circ Syst Signal Process*, 17(2):137-164. https://doi.org/10.1007/BF01202851

Velichko A, 2019. A method for evaluating chimeric synchronization of coupled oscillators and its application for creating a neural network information converter. *Electronics*, 8(7):756. https://doi.org/10.3390/electronics8070756

Velichko A, Belyaev M, Putrolaynen V, et al., 2018a. Modeling of thermal coupling in VO_2-based oscillatory neural networks. *Sol-State Electron*, 139:8-14. https://doi.org/10.1016/j.sse.2017.09.014

Velichko A, Belyaev M, Putrolaynen V, et al., 2018b. Thermal coupling and effect of subharmonic synchronization in a system of two VO_2 based oscillators. *Sol-State Electron*, 141:40-49. https://doi.org/10.1016/j.sse.2017.12.003

Wang TS, Roychowdhury J, 2019. OIM: oscillator-based Ising machines for solving combinatorial optimisation problems. Proc 18th Int Conf on Unconventional Computation and Natural Computation, p.232-256. https://doi.org/10.1007/978-3-030-19311-9_19

Xu XX, Zheng CG, Zhang T, 2013. Reduction in LFP cross-frequency coupling between theta and gamma rhythms associated with impaired STP and LTP in a rat model of brain ischemia. *Front Comput Neurosci*, 7:27. https://doi.org/10.3389/fncom.2013.00027

Zheng CG, Bieri KW, Hsiao YT, et al., 2016. Spatial sequence coding differs during slow and fast gamma rhythms in the hippocampus. *Neuron*, 89(2):398-408. https://doi.org/10.1016/j.neuron.2015.12.005